Bearing capacity of large-diameter open caissons embedded in sand

Brian Sheil[1]* and Jack Templeman[1]

[1]Department of Engineering Science, University of Oxford, Parks Road, Oxford OX1 3PJ, UK

*Corresponding author. Email: brian.sheil@eng.ox.ac.uk.

Tables: 1

Figures: 16

ABSTRACT

Large-diameter open caissons are an increasingly common means of constructing underground storage and attenuation tanks as well as launch and reception shafts for tunnel boring machines. The caisson walls typically feature a tapered base, referred to as the 'cutting face', to aid the sinking process by reducing the vertical soil reaction. The primary aim of this paper is to explore the influence of the caisson cutting face inclination angle on the vertical soil reaction in sand. Both finite element limit analysis and finite element analysis are adopted for this purpose. The effects of cutting face roughness, external embedment depth, and caisson radius are also investigated. The results show that the influence of the cutting face inclination angle on the bearing capacity is highly dependent on both the soil friction angle and the roughness of the cutting face. A reduction in the caisson radius is also shown to cause a significant increase in the vertical soil reaction. The numerical output is used to inform the development of a new closed-form analytical approach amenable for use in routine design. The design method is shown to provide a high-fidelity representation of the numerical output.

INTRODUCTION

Deep shafts and caissons have a wide range of geotechnical applications including foundation solutions, storage and attenuation tanks, and launch and reception shafts for tunnel boring machines. A common construction procedure is to 'sink' monolithic reinforced concrete caissons into the ground using the self-weight of the caisson walls. A key feature of the caisson wall cross-section is a tapered base, typically known as the 'cutting face'. This resembles an inclined ring footing and is used to promote sinking by reducing the vertical bearing resistance of the soil (Royston et al. 2020). An accurate estimation of this resistance is an essential element of the design process: over-estimation can lead to uncontrolled and dangerous sinking whereas under-estimation can result in failure to reach formation level (Sheil et al. 2018).

The widely used Terzaghi (1943) bearing capacity theory provides the following expression for calculating the bearing capacity of a strip footing:

$$V/A = cN_{\mathrm{c}} + qN_{\mathrm{q}} + \frac{1}{2}\gamma BN_{\gamma} \quad (1)$$

where V is the vertical bearing capacity force, A is the footing area, c is the soil cohesion, q is the surrounding surcharge, γ is the unit weight of the soil and N_{c}, N_{q} and N_{γ} are the dimensionless bearing capacity factors providing the contributions of c, q and γ respectively. Many investigators have sought to develop more accurate solutions for the bearing capacity factors using numerical techniques such as finite element analysis (FEA; Goss and Griffiths 2001, Gourvenec 2007, Georgiadis 2010), method of characteristics (e.g. Smith 2005, Houlsby and Martin 2003) and finite element limit analysis (FELA; Merifield et al. 1999, Salgado et al. 2004, Lyamin et al. 2007, Sloan 2013). Equation (1) is typically extended to footings founded below the ground surface and/or subjected to oblique loads through the use of additional depth and load inclination factors respectively e.g. Meyerhof (1951, 1963), Brinch Hansen (1970), De Beer (1970), Vesic (1973), Sastry and Meyerhof (1987), Van Baars (2014). Similarly, 'shape' factors have been used to compute the bearing capacity of

41 foundations with alternative geometries e.g. Michalowski (2001), Lyamin et al. (2007),
42 Gourvenec (2007), Taiebat and Carter (2010).

43 The vertical bearing capacity of ring footings has been studied using various experimental
44 and numerical techniques in both cohesionless (e.g. Saha 1978, Saran et al. 2003, Kumar
45 and Ghosh 2005, Boushehrian and Hataf 2003, Zhao and Wang 2008, Choobbasti et al.
46 2010, Benmebarek et al. 2012, Kumar and Chakraborty 2015) and cohesive soils (e.g. Lee
47 et al. 2016, Benmebarek et al. 2017). However, the influence of the footing inclination angle
48 on the bearing capacity has received much less attention. Hansen (1970) documented one
49 of the earliest uses of 'base factors' to modify the Terzaghi bearing capacity equation to
50 account for the influence of an inclined footing base. More recently, Royston et al. (2016)
51 and Chavda et al. (2019) have explored the influence of the base inclination angle on ring
52 footings embedded in sand (for open caisson applications) using small-scale laboratory
53 testing. The present review of the literature identifies a lack of robust design calculations for
54 the bearing capacity of a caisson cutting face in cohesionless soil.

55 To address these uncertainties, this paper presents the results of a suite of finite element
56 limit analyses of the vertical penetration behaviour of a caisson cutting face in drained soil.
57 Parameters considered in the modelling include the soil friction angle, the inclination and
58 roughness of the caisson cutting face, the external embedment depth and the caisson
59 radius. A limited number of finite element analyses were also undertaken to explore the
60 influence of soil non-associativity on the vertical bearing capacity. The FELA output is used
61 to inform the development of closed-form analytical expressions amenable for use in routine
62 design.

63

64 **PROBLEM DEFINITION**

65 Figure 1 defines the problem and notation for this study. The geometry of the caisson cutting
66 face is described by the angle of inclination, β, embedded width, *B*, which isequal to the total

wall width, and internal radius, R. The caisson is considered embedded in homogeneous drained soil with unit weight γ′, friction angle ϕ′, dilation angle ψ′ and cohesion c = 0. In this study, the internal soil level is assumed to always remain at the top of the taper face to reflect the soil excavation process inside the caisson; the external embedment depth, relative to the internal soil surface level, is given by h. The cutting face roughness is defined by a roughness factor, α, such that the interface friction angle, δ, is given by tan δ = α tanϕ′ (Cassidy and Houlsby 2002) where values of α of 0 and 1 denote a fully smooth and fully rough interface respectively. The vertical and horizontal reaction exerted by the soil on the cutting face is V and H respectively. Bearing capacity results are presented in the form of a dimensionless factor, N', henceforth:

$$N' = 2\frac{V/A}{\gamma' B} \tag{2}$$

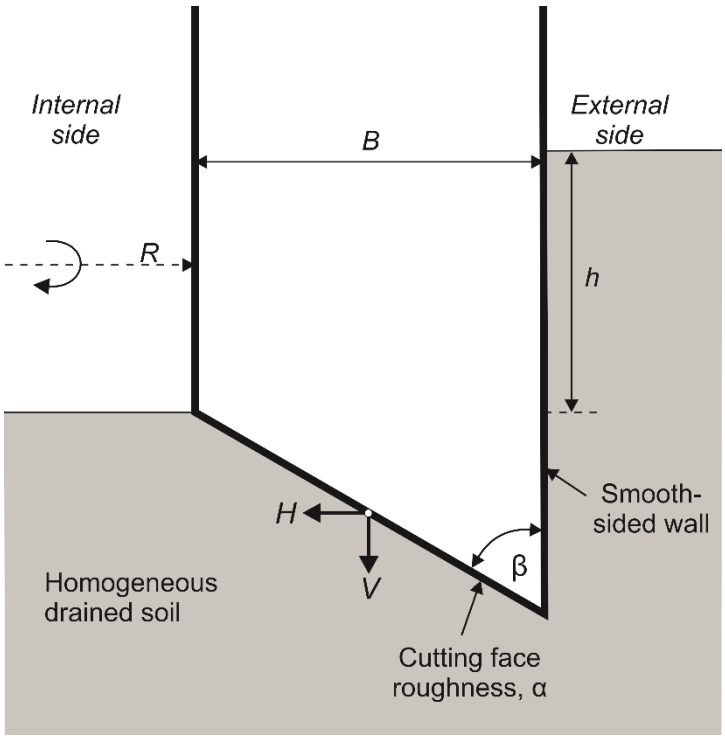

Fig. 1 Problem definition.

FINITE ELEMENT LIMIT ANALYSIS

The majority of the numerical analyses described in this paper were performed using the FELA software package Optum G2 (Krabbenhoft et al. 2016). In these analyses, the soil was modelled as a rigid-plastic material obeying the Mohr-Coulomb (MC) failure criterion while the caisson was modelled as a rigid body. For each problem, an analysis was conducted using strict lower- (LB) and upper-bound (UB) plasticity solutions. The LB analyses used triangular elements with a linear variation in stresses between corner nodes such that yield conditions are enforced at the three corner nodes. The UB analyses used triangular elements with quadratic interpolation of displacements and linear interpolation of stresses within each element. This process allows a rigorous bracketing of the exact collapse loads where the error can be defined as follows:

$$error(\%) = \pm \frac{UB - LB}{(UB + LB)} \tag{3}$$

In all analyses the error was less than ±5% and the final collapse loads were obtained by averaging the LB and UB collapse multipliers at the end of the analysis. Each model was initially uniformly discretised with 1,000 elements. The total number of elements at the end of the analysis varied up to a maximum of 50,000 elements after seven rounds of adaptive meshing, based on the distribution of plastic shear dissipation. The resulting concentration of elements in the mesh reflects the characteristics of the soil failure mechanisms.

FINITE ELEMENT ANALYSIS

Finite element model

A limited number of FEA calculations were also completed to explore the influence of soil non-associativity on the bearing capacity of the cutting face using the commercial software Abaqus/Standard (SIMULIA 2017). The soil is defined as a two-dimensional domain meshed with six-node quadratic plane strain triangular elements (CPE6). The caisson section is

105 defined using a separate body meshed with two-node rigid (R2D2) elements tied to a
106 reference node to create a rigid body. The interaction between the soil and caisson section
107 is modelled using a surface-to-surface finite-sliding formulation. The shear strength of the
108 interface is defined using classical isotropic Coulomb friction with zero dilatancy.
109 *Material model*

110 The adopted constitutive model is linear isotropic elasticity with perfect plasticity, governed
111 by a rounded approximation to the MC yield surface. The yield criterion used in this study is
112 based on the MC approximation presented by Abbo et al. (2011), as shown in Fig. 2. This
113 surface uses hyperbolic rounding in the meridional plane to eliminate the tip discontinutity
114 (Fig. 2(a)) and trigonometric rounding in the octahedral plane to smooth the yield crtierion in
115 the vicinity of the edge discontinuties (Fig. 2(b)). This gives a conservative approximation
116 that is continuous in both its gradient and gradient derivative at all stress states and
117 therefore provides a robust numerical implementation. The closeness-of-fit between the
118 approximate surface and the 'parent' conventional MC surface (i.e. for the same *c* and ϕ'
119 values) is governed by (a) the meridional rounding parameter, a, which defines the distance
120 between the tip of the MC criterion and the hyperbolic approximation (see Fig. 2(a)), and (b)
121 the transition angle, θ_T, which is the Lode angle that defines the transition from exact
122 conventional MC behaviour to trigonometric rounding in the octahedral plane (see Fig. 2(b)).
123 The plastic potential of the constitutive model in this study is assumed to be of the same
124 form as the yield function, except that ϕ' is replaced with ψ'.
125
126

(a)

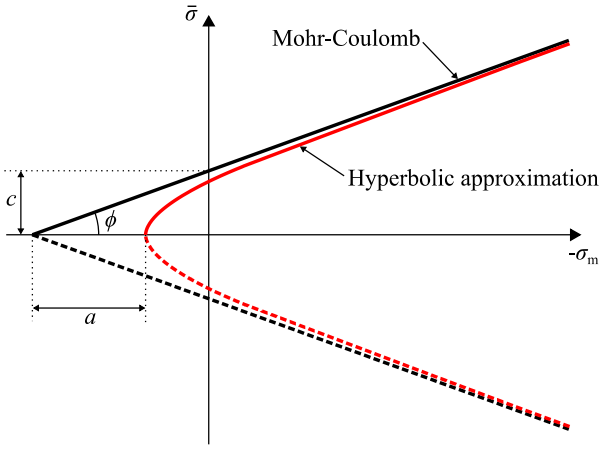

(b)

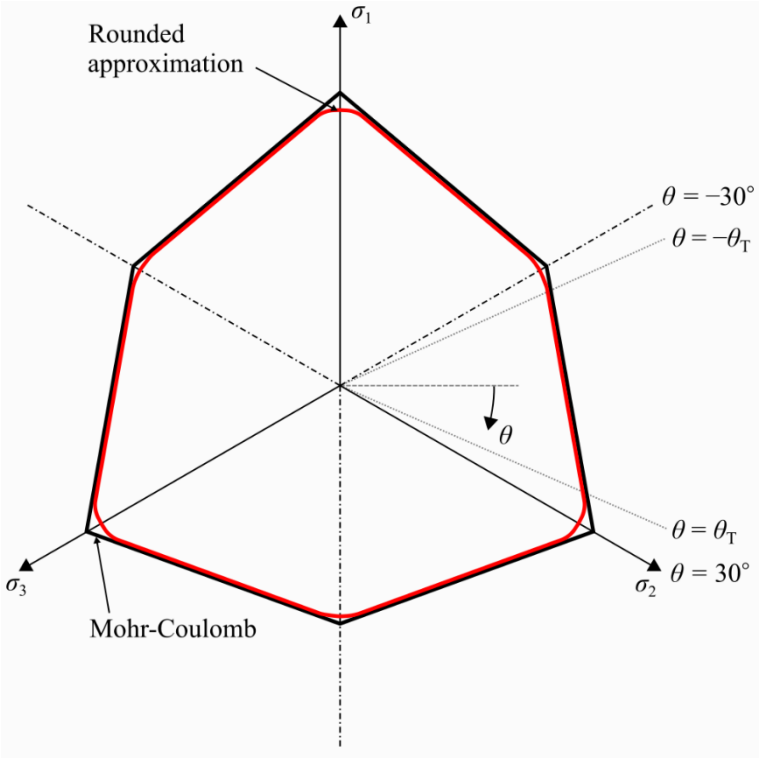

Fig. 2 Smooth approximation to the MC criterion superimposed on the conventional MC surface: (a) Meridional section showing the hyperbolic approximation to eliminate the tip discontinuity, (b) Octahedral section showing the trigonometric rounding to smooth the edge discontinuities.

The soil material model is implemented in Abaqus/Standard using a user-defined material subroutine (UMAT) written in Fortran. The adopted numerical stress integration approach is based on the explicit modified Euler scheme, with adaptive sub-stepping and error control, presented by Sloan et al. (2001). The present approach uses the algorithms proposed by Sloan et al. (2001) to identify yield surface intersection during elastic-to-plastic transitions and to handle elastoplastic transitions. Stress correction is also performed to return the updated stresses to the yield surface after each substep if the yield tolerance is exceeded. In this study the tolerances on the yield function evaluation and stress error (*FTOL* and *STOL* respectively in Sloan et al. (2001)) were both taken to be 1×10^{-6}.

Adaptive remeshing

The FEA calculations in this study were performed using an adaptive mesh refinement process, as described in Martin (2011) and summarised in Fig. 3. The initial iteration analysis starts with the creation of a planar straight line graph (PSLG) that represents the specified geometry of the problem. The open source program Triangle (Shewchuk, 1996, 2002) is used to generate a uniform 2D unstructured triangular mesh of the PSLG using conforming constrained Delaunay triangulation; these mesh details are extracted and incorporated into an Abaqus input file. The modelling procedure then enters a series of remeshing iterations, in which the soil domain mesh is progressively refined based on the previous FEA results. In this work, the remeshing scheme seeks to equalise the integral of the maximum principal mechanical strain rate over all elements in the mesh. In each iteration, Triangle is called to remesh the previous mesh based on calculated target area values, before a new FEA input file is generated and supplied to Abaqus; in this study, four rounds of remeshing was sufficient for the FEA calculations.

NUMERICAL MODELLING

Modelling preliminaries

In all analyses, the soil domain was sized such that it comfortably contained the soil failure mechanism for all soil/caisson parameter combinations considered. The lateral boundaries were restricted from movement normal to the respective surface whereas the bottom boundary was restrained from movement in all directions. The analyses assume that the space above the cutting face is occupied by a rigid, smooth-sided wall due to the use of interface lubrication during caisson sinking (Royston et al. 2016, 2020). Therefore, only the roughness of the cutting face is considered in the subsequent analyses. The following stages of analysis were adopted in the modelling:

I. Initialisation of soil stresses. This was achieved through the application of gravity in the FELA calculations; the FEA involved application of a negative body force to the soil domain in the vertical direction followed by a geostatic step to equilibrate soil stresses.

II. Wished-in-place installation of a weightless, rigid cutting face to an embedded width of B = 2 m in drained soil with $\gamma' = 1$ kN/m^3, friction angle ϕ', dilation angle ψ' and external soil depth, h. Additional parameters used specifically in the FEA modelling include the soil Young's modulus, $E = 5 \times 10^7$ MPa, Poisson's ratio, $v = 0.3$ and rounding parameters $a = 0.1c/\tan(\phi')$ and $\theta_T = 29°$. Note that an unrealistically large E is chosen to approximate rigid-plastic soil behaviour and the exact value of E does not influence the resulting collapse load. A small value for c (typically 5×10^{-4} kPa) was adopted for numerical stability in the FEA calculations. The footing was restrained in all three degrees of freedom during this calculation phase.

III. Application of a downward load multiplier (FELA) or prescribed displacement (FEA) until failure is achieved. During this step, only vertical movement was allowed. The treatment of the penetration problem in this way tacitly assumes that the caisson behaves as a rigid body and remains vertical during the sinking process.

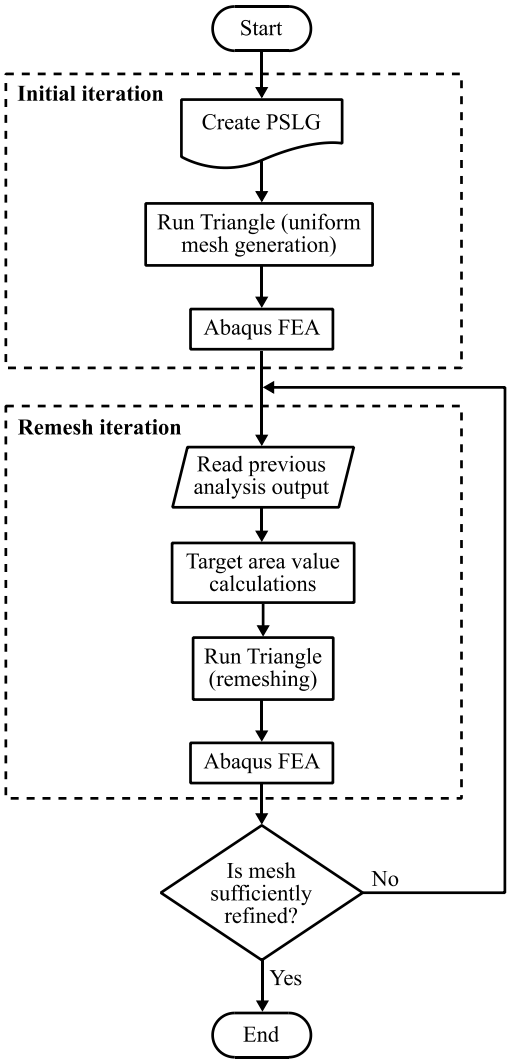

Fig. 3 Overview of the adaptive remeshing FEA procedure.

Validation

A validation exercise was undertaken to confirm that the adopted FELA and FEA modelling procedures produced correct results for the vertical bearing capacity of a surface strip footing with no applied ground surface pressure. Figure 4 plots the FELA- and FEA-calculated values of N' (as defined by equation (2)) as a function of ϕ'. Solutions reported by Hijaj et al. (2005) are also plotted for comparison. It can be observed that the present FELA and FEA solutions are in excellent agreement with the Hijaj et al. (2005) solutions giving confidence in the present modelling. Figure 5 also compares the mesh generated using the custom FEA adaptive remeshing strategy described by Fig. 3 with the mesh generated using Optum's adaptive mesh implementation. It can be qualitatively observed that both meshes

are in very good agreement. After several iterations of adaptive refinement, the elements become increasingly refined in regions where the intensity of maximum principal strain rate is greatest. This results in velocity discontinuities appearing as dark bands of high concentration of small elements, regions of diffuse plastic shearing undergo intermediate levels of refinement and rigid blocks remain largely unrefined (Martin, 2011).

(a)

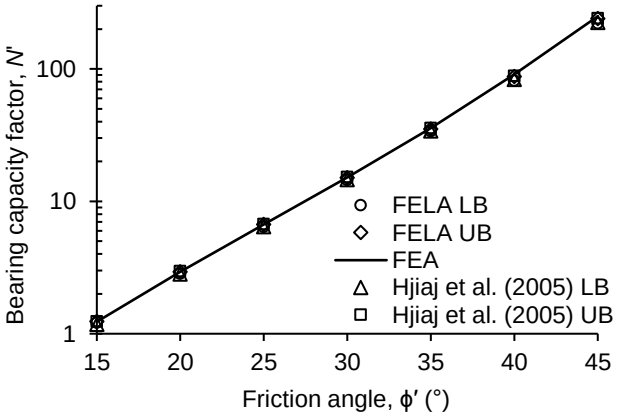

(b)

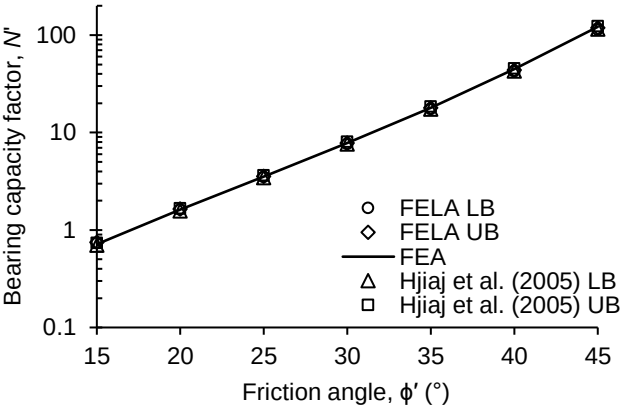

Fig. 4 Validation of bearing capacity calculations determined using present FELA and FEA models through comparisons to FELA solutions previously documented by Hjiaj et al. (2005) for a flat strip footing with a (a) rough and (b) smooth interface; ψ′ = ϕ′.

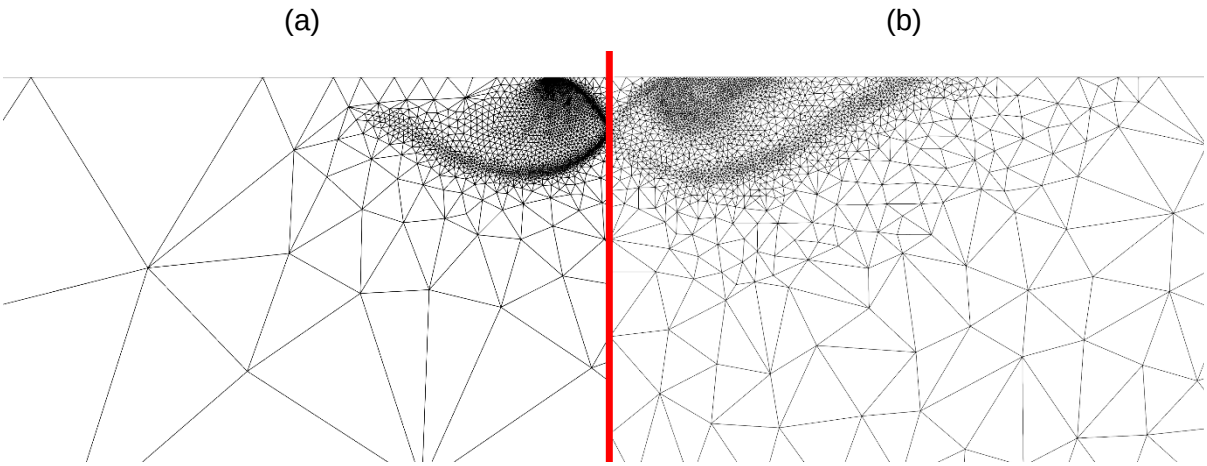

Fig. 5 Exemplar finite element meshes obtained for a conventional rough flat strip footing on a level bed of $\phi' = 30°$ soil after four rounds of adaptive remeshing (~7000 elements): (a) FELA UB analysis (based on shear dissipation rates), (b) FEA (based on maximum principal strain rates); $\psi' = \phi'$.

Overview of numerical study

All 6300 combinations of the following five dimensionless parameters were explored using FELA:

(a) Soil friction angle, ϕ': 15°, 20°, 25°, 30°, 35°, 40°, 45°;

(b) Cutting face inclination angle, β: 90°, 75°, 60°, 45°, 30°;

(c) Cutting face roughness, α: 0, 0.25, 0.5, 0.75, 1.0;

(d) Dimensionless external embedment depth, *h/B*: 0, 2.5, 5, 7.5, 10, 15;

(e) Dimensionless caisson radius, *B/R:* 0.5, 0.4, 0.3, 0.2, 0.1, 0 (plane strain).

In addition, a limited number of FEA calculations were undertaken to explore the role of soil non-associativity on the bearing capacity of a caisson cutting face; parameters specific to the FEA modelling are listed in Table 1.

Table 1 Parameters adopted for the limited number of FEA calculations

Parameter	Value
Cutting face inclination, β	30°, 45°, 60°, 75°, 90°
Cutting face roughness	Fully rough

Soil friction angle, ϕ'	40°
Soil dilation angle, ψ'	40°, 20°, 10°

NUMERICAL RESULTS

Influence of cutting face inclination

The FELA-calculated influence of β on N' is presented in Fig. 6 considering both a rough (α = 1) and smooth (α = 0) cutting face and values of ϕ' ranging between 15° and 45° for a level soil surface (h/B = 0). Considering first the results for α = 1 (Fig. 6(a)), a reduction in β causes an increase in N' for all values of ϕ' where an approximately log-linear relationship can be observed. These data are re-plotted in Fig. 6(b) except that values of N' have now been normalised by their corresponding flat footing values, $N'_{\beta=90^\circ}$. It can be seen that the gradient of $N'/N'_{\beta=90^\circ}$ with respect to β is a function of ϕ': β has less of an influence on the vertical bearing capacity for high-ϕ' soil.

Similar observations may be deduced from the corresponding figures for α = 0 (Figs. 6(c) and 6(d)). In this case, the relationship between $N'/N'_{\beta=90^\circ}$ and β is slightly non-linear. Interestingly, a steepening of the cutting face (reduction in β) causes an increase and reduction in the bearing capacity for small and large values of ϕ' respectively. To further explore the source of this incongruity, soil failure mechanisms corresponding to β = 90°, 75° and 30° and ϕ' = 15° and 45° are presented in Fig. 7. It can be seen that for ϕ' = 15° a reduction in β causes an increase in the size of the failure mechanism due to the greater embedded depth of the caisson vertex (see Figs. 7(a) – 7(c)). Conversely, while a reduction in β from 90° to 75° causes an increase in the size of the failure mechanism on the internal side for ϕ' = 45°, this is balanced by the reduction in the mechanism on the external side (see Figs. 7(d) and 7(e)). A further reduction in β to 30° causes the failure mechanism to move entirely to the internal side.

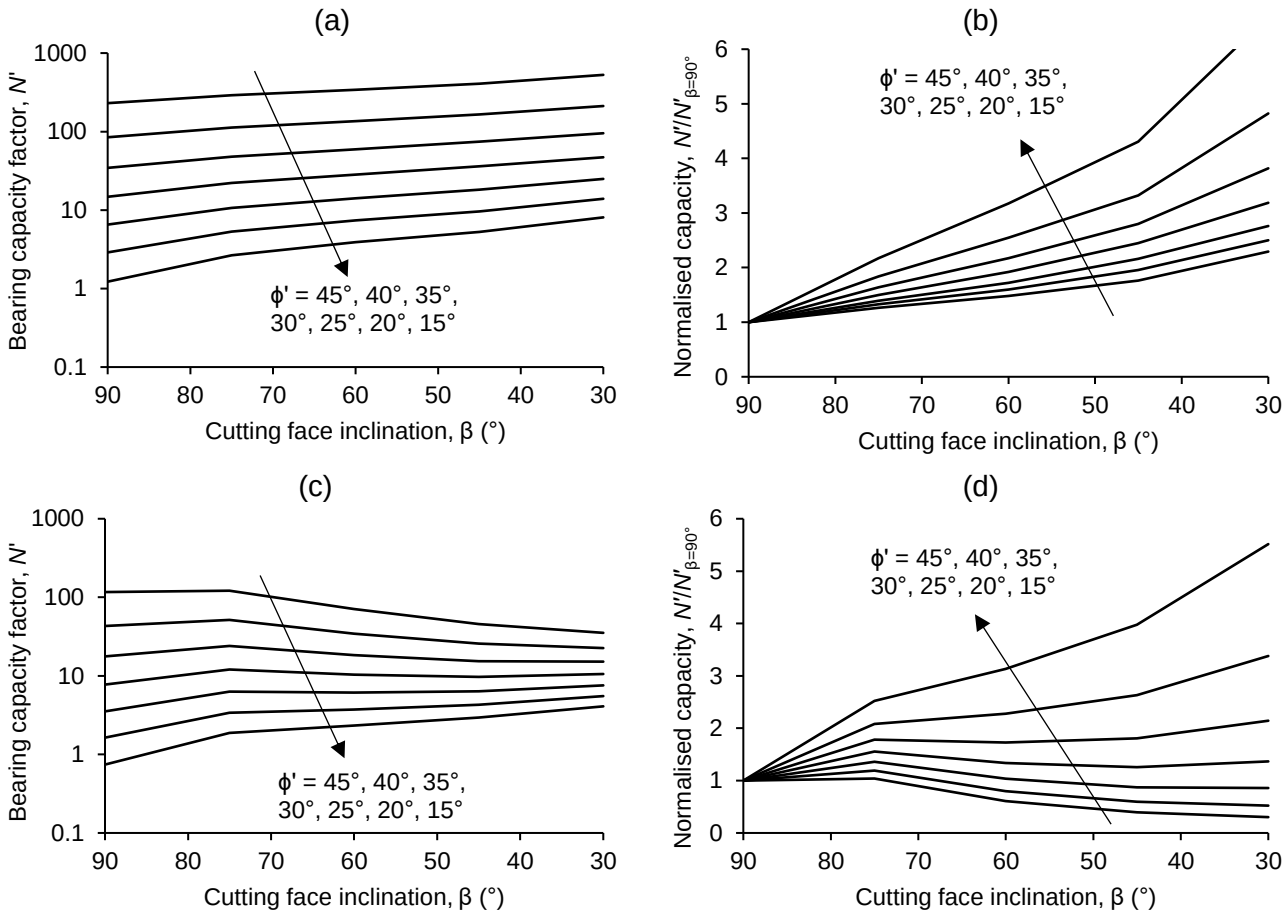

Fig. 6 FELA-calculated influence of the cutting face inclination angle on vertical bearing capacity for values of ϕ′ ranging between 15° and 45°: (a) N' (rough cutting face), (b) bearing capacity normalised by corresponding flat footing values, $N'/N'_{\beta=90°}$ (rough cutting face), (c) N' (smooth cutting face), (d) bearing capacity normalised by corresponding flat footing values, $N'/N'_{\beta=90°}$ (smooth cutting face); $h/B = 0$, $B/R = 0$ (plane strain), $\psi' = \phi'$.

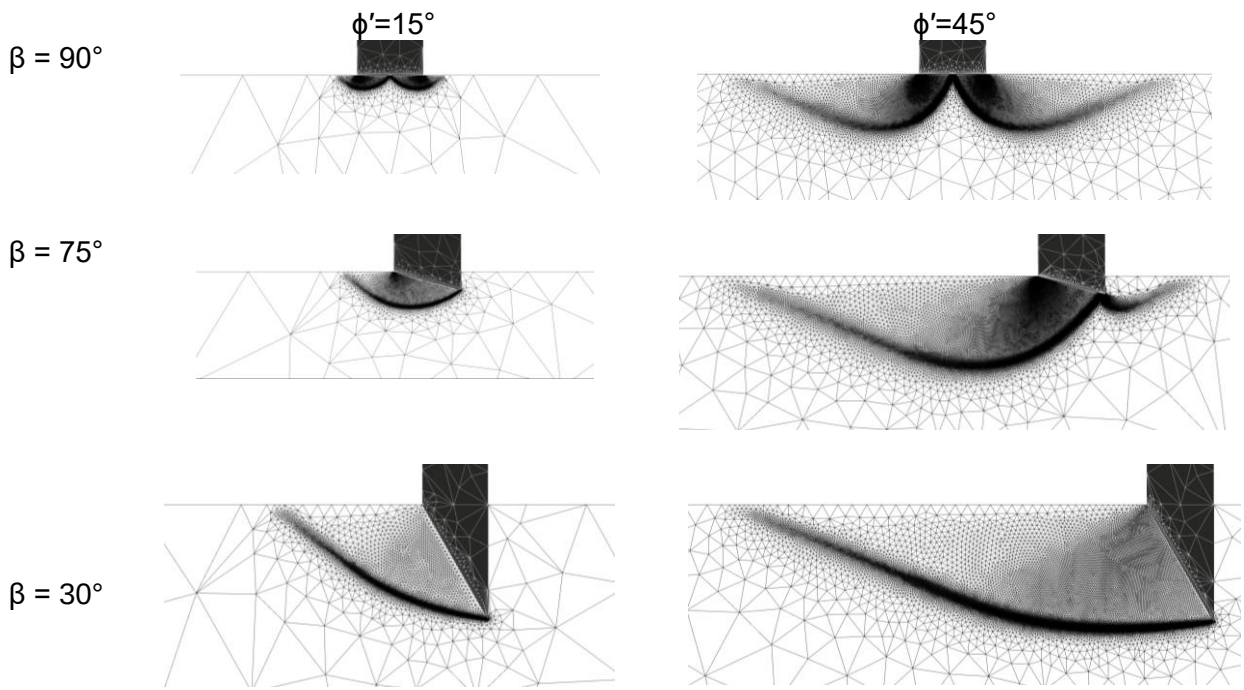

Fig. 7 FELA-calculated influence of β on soil failure mechanisms for a smooth cutting face using mesh refinement from the UB analysis to reveal slip line fields; flat surface (h = 0), B/R = 0 (plane strain), ψ′ = ϕ′.

Influence of soil non-associativity

In Fig. 8, the role of soil non-associativity on the non-dimensional load-displacement response of a β = 75° rough cutting face is investigated using FEA. Also superimposed on this plot are the corresponding FELA results (ψ′ = ϕ′ only). It can be seen that for the associated flow analyses, there is good agreement between the FELA and FEA calculations (~5% difference). A reduction in ψ′ (non-associated flow) causes oscillations in the vertical load which is exacerbated by an increase in ϕ′. These features of non-associated flow behaviour are well-documented and do not undermine the validity of the present FEA results (De Borst and Vermeer 1984, Vermeer 1990, Drescher and Detournay 1993).

For the non-associated flow analyses, collapse loads are selected as the maximum load that occurred during the analysis, in accordance with the approach taken by Loukidis and Salgado (2009). These values are plotted as a function of β in Fig. 9. Select FELA results

from Fig. 6 have also been plotted for comparison. It can again be seen that there is good agreement between the FEA and FELA results for the associated flow analyses (ψ′ = ϕ′). For non-associated flow (ψ′ < ϕ′), there is a significant reduction in N', particularly for smaller values of ψ′. From the FEA calculations presented in Fig. 10, a reduction in ψ′ causes a change in the shape of the failure mechanism as well as a reduction in their size. Another important consequence of non-associativity is the presence of thin localised shear bands.

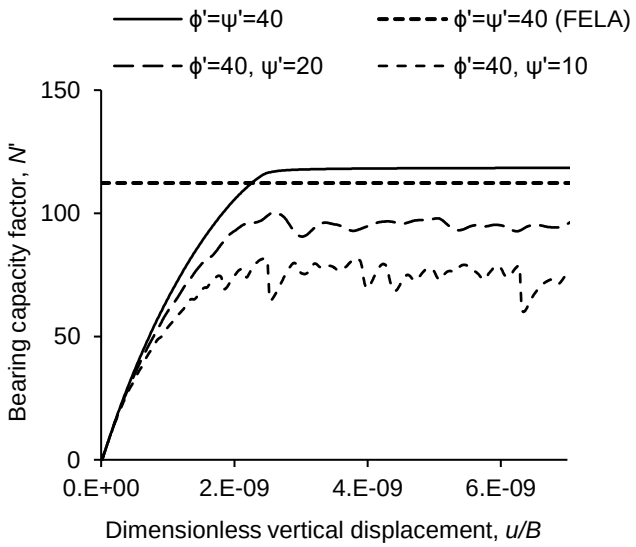

Fig. 8 FEA-calculated influence of soil associativity on the dimensionless load-displacement response of a β = 75° rough cutting face; flat surface (h = 0), B/R = 0 (plane strain).

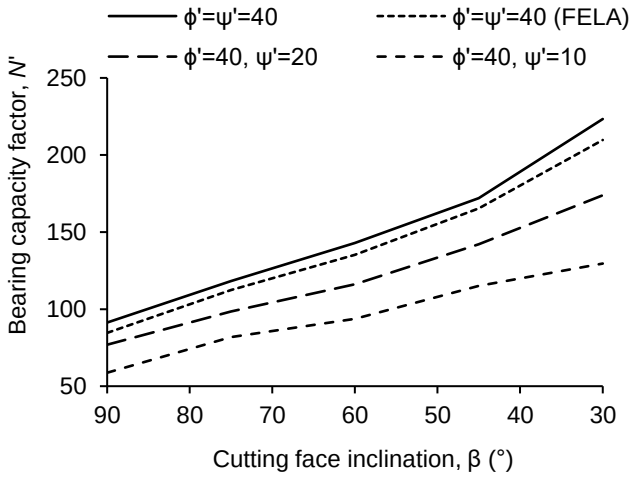

Fig. 9 FEA-calculated influence of soil non-associativity on the relationship between N' and β; rough cutting face, flat surface (h = 0), B/R = 0 (plane strain).

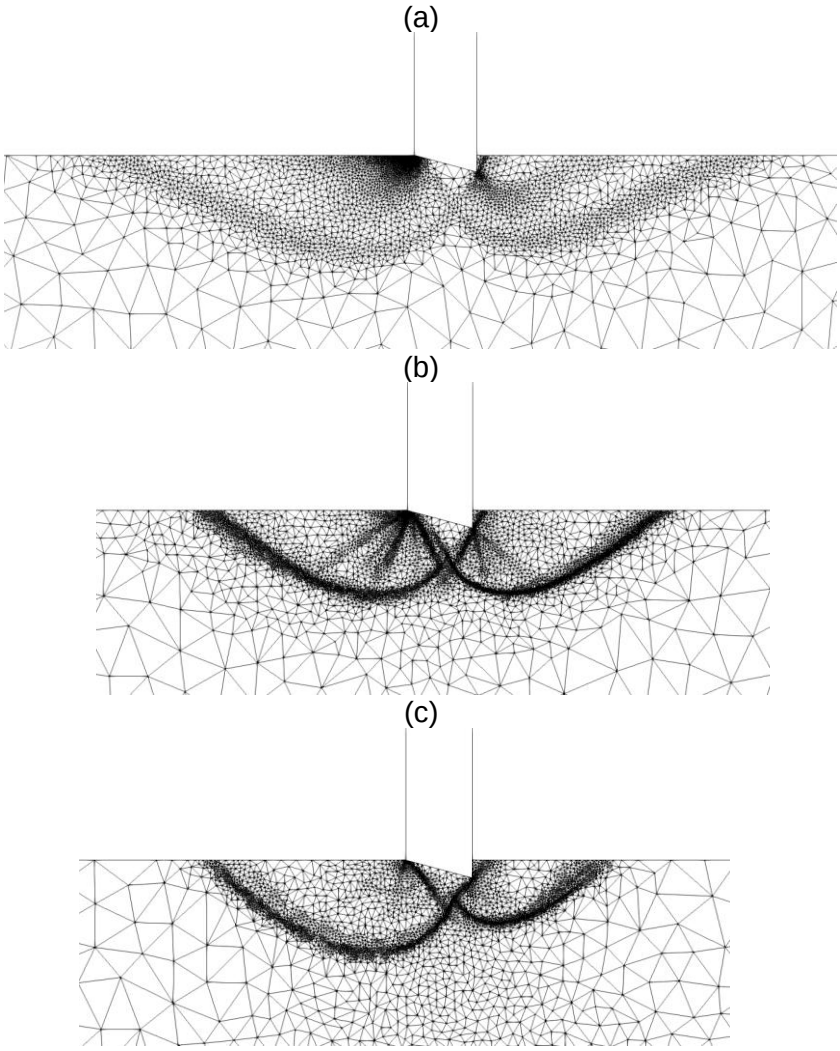

Fig. 10 FEA-calculated influence of non-associativity on soil failure mechanisms for ϕ′ = 40°: (a) ψ′ = 40°, (b) ψ′ = 20°, (c) ψ′ = 10°; β=75°, rough cutting face, flat surface (*h* = 0), *B*/*R* = 0 (plane strain).

Influence of external embedment depth

FELA calculations of the influence of the caisson external embedment depth, *h,* on the vertical bearing capactity are plotted in Fig. 11 where N' is normalised by the corresponding flat surface values, $N'_{h=0}$. For the sake of clarity, only salient values of β and ϕ′ are considered in this and subsequent figures. It can be observed that the influence of *h*/*B* on the vertical bearing capacity is highly dependent on both the cutting face inclination angle and the soil friction angle. For example, an increase in *h*/*B* causes a signficant increase in

bearing capacity for ϕ′ = 45° and β = 75° whereas the ϕ′ = 20° analyses show a negligible influence of *h/B* regardless of the adopted value of β. These results indicate that an increase in *h*/*B* has a significant influence on bearing capacity for high-ϕ′ soil and flatter cutting face angles (high-β). For the ϕ′ = 45° analyses, there also appears to be a critical embedment depth, h_{crit}, beyond which a further increase in *h* has a negligible effect on *N*′. The value of h_{crit} appears independent of β where a value of h_{crit}/B of approximately 10 is obtained for ϕ′ = 45°. Moreover, *h* has a much greater influence on bearing capacity for α = 1 (Fig. 11(a)) compared to α = 0 (Fig. 11(b)).

(a)

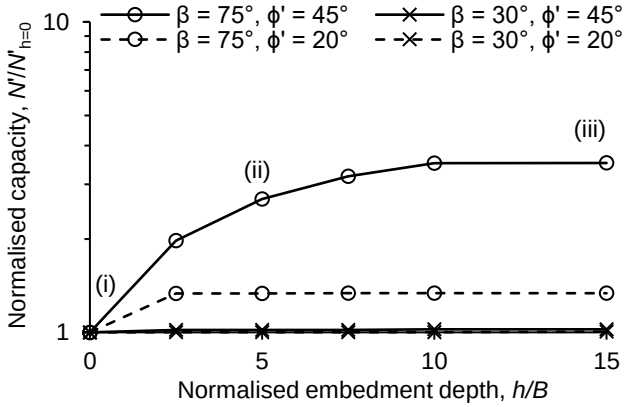

(b)

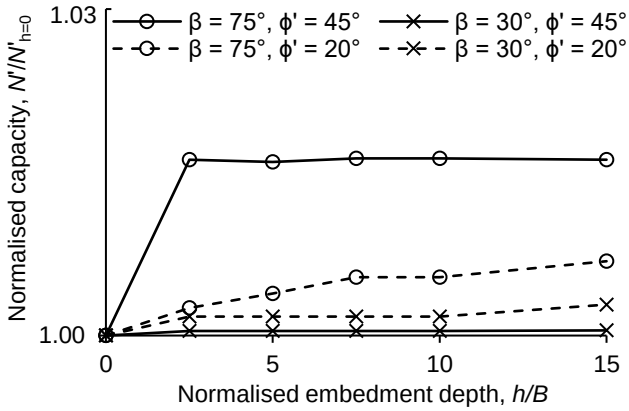

Fig. 11 FELA-calculated influence of external embedment depth on the vertical bearing capacity normalised by the corresponding flat surface values, $N/N_{h=0}$ for (a) rough, and (b) smooth cutting faces; *B*/*R* = 0 (plane strain), ψ′ = ϕ′.

The underpinning mechanism for the occurrence of h_{crit} is explored via the soil failure mechanisms presented in Figs. 12(a) – 12(c), corresponding to points (i) to (iii) marked on Fig. 11(a). Aside from increasing the confining stress of acting on the soil shear failure planes, an increase in *h*/*B* from 0 to 5 also causes an extension of the soil failure mechanism to the external side of the caisson wall. However, it can be seen that an increase in *h/B* from 5 to 15 causes the soil failure mechanism to be confined to the internal side only thus any further increases in embedment causes a negligible increase in capacity.

(a)

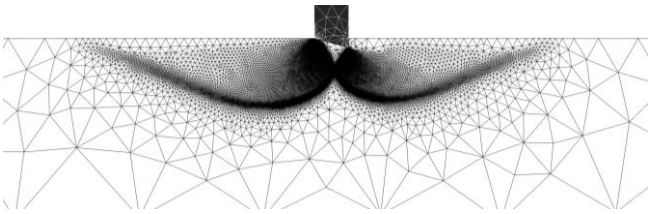

(b)

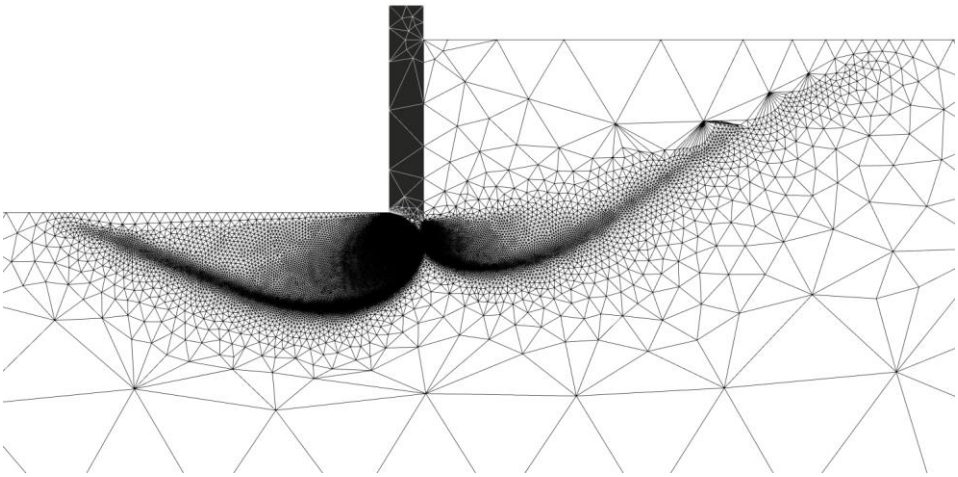

(c)

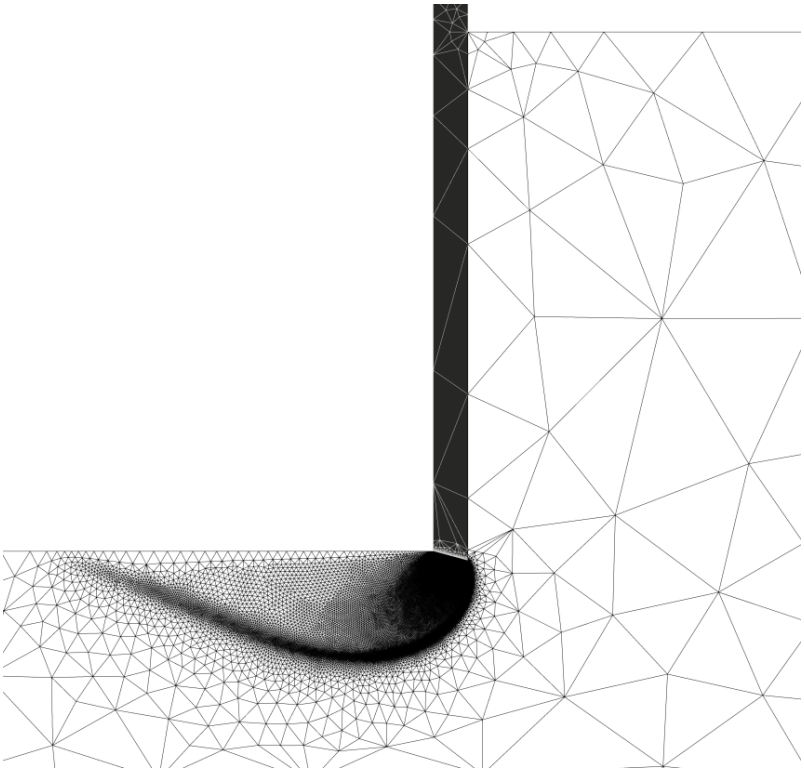

Fig. 12 FELA-calculated influence of the external embedment depth on soil failure mechanisms using the refined mesh from an UB analysis to reveal slip line fields: (a) h/B = 0, (b) h/B = 5, (c) h/B = 15; $\phi' = 45°$, $\beta = 75°$, rough cutting face, B/R = 0 (plane strain), $\psi' = \phi'$.

Influence of caisson radius

Figure 13 presents the FELA-calculated vertical bearing capacity normalised by the corresponding plane strain values plotted as a function of the reciprocal of the dimensionless caisson radius (B/R). In general, the development of the logarithm of $N'/N'_{R=\infty}$ appears to be a linear response to an increase in B/R for both $\alpha = 1$ (Fig. 13(a)) and $\alpha = 0$ (Fig. 13(b)). In all cases, an increase in B/R causes an increase in the normalised bearing capacity due to an increase in radial stress (and therefore confining stress). However, the gradients of the curves presented in Fig. 13 appear to be dominated by ϕ': high-ϕ' soil causes a significant dependency of N' on B/R regardless of cutting face roughness. In contrast, β has less of an influence on this relationship. For smaller caisson radii (larger values of B/R), an increase in β from 30° to 75° causes a reduction in $N'/N'_{R=\infty}$ for $\alpha = 1$. From the corresponding failure

mechanisms presented in Figs. 14(a) and 14(b) respectively, it can be observed that (i) both failure mechanisms now extend to the external side (c.f. Fig. 12(c)) and (ii) the mechanism corresponding to β = 30° extends further downwards into stronger soil causing a greater contribution to the bearing capacity. Conversely, an increase in β from 30° to 75° causes a marginal increase in $N'/N'_{R=\infty}$ for α = 0 due to the flatter inclination angle (see Fig. 13(b)).

(a)

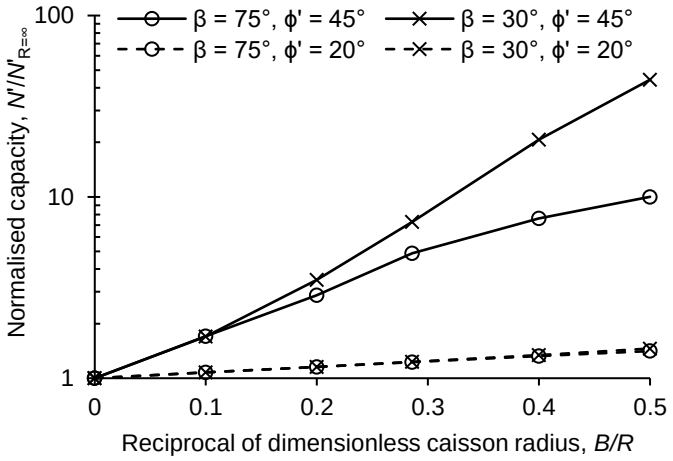

(b)

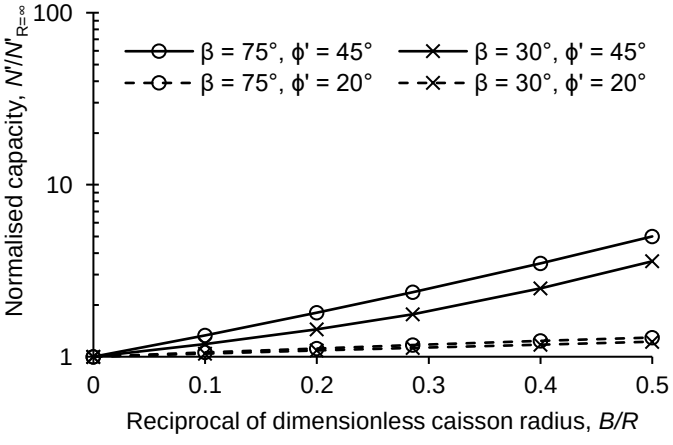

Fig. 13 FELA-calculated influence of the dimensionless caisson radius *B/R* on the vertical bearing capacity normalised by the corresponding plane strain values, $N'/N'_{R=\infty}$ for (a) rough and (b) smooth cutting faces; *h/B* = 15, ψ′ = ϕ′.

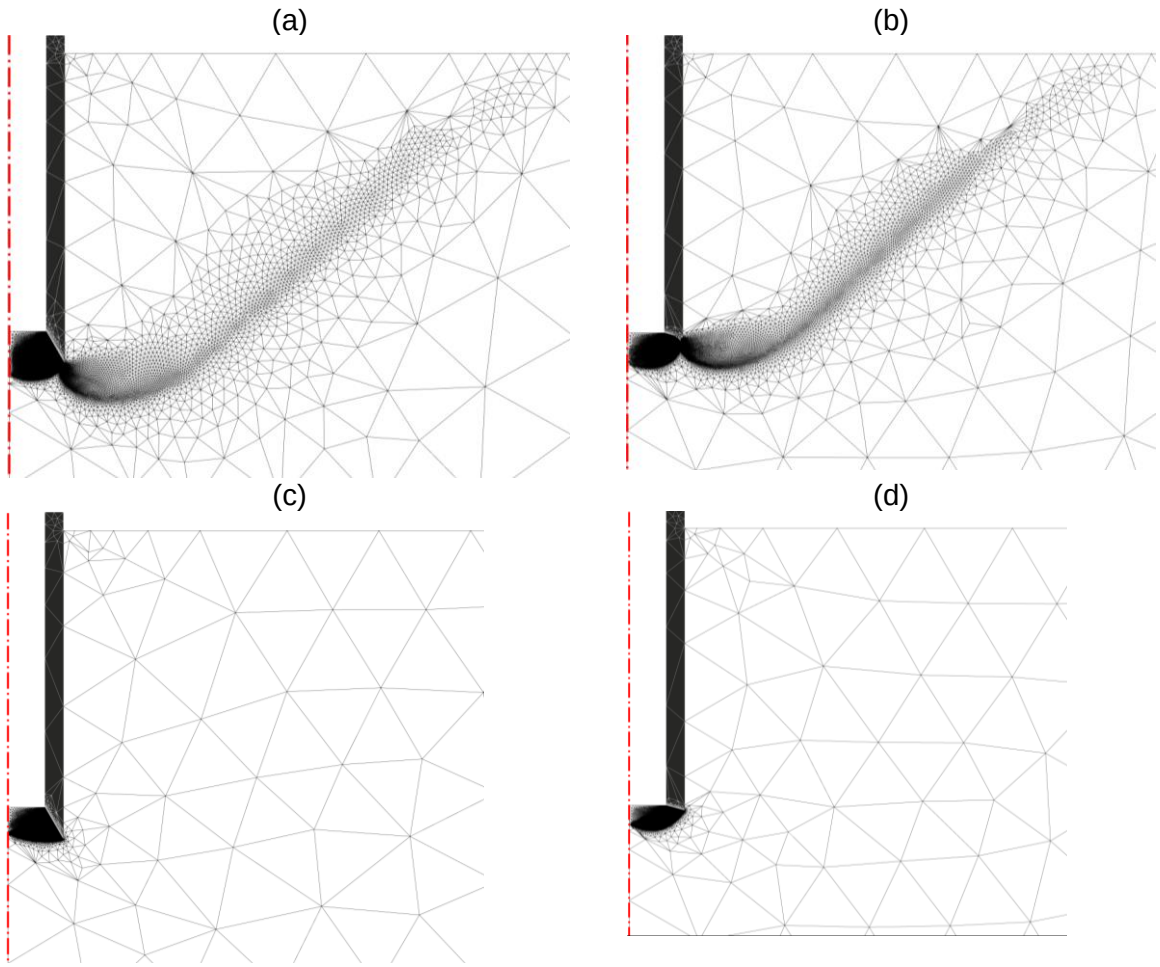

Fig. 14 FELA UB calculations of the soil failure mechanisms for a small-diameter caisson (*B*/*R* = 0.5): (a) β = 30° and α = 1, (b) β = 75° and α = 1, (c) β = 30° and α = 0, (d) β = 75° and α = 0; *h*/*B* = 15, ϕ′ = 45°, ψ′ = ϕ′.

DESIGN CALCULATION FOR CAISSON SINKING IN SAND

Design method development

While direct numerical analyses of geotechnical problems are becoming more commonplace, simplified design approaches remain an integral part of preliminary design. This is particularly the case for the design of large-diameter open caissons where the selection of the cutting shoe geometry is a construction detail and therefore most commonly rests with the contractor. The FELA results presented in this paper were therefore used to inform the development of closed-form analytical equations amenable for use in routine design. Only the deep condition (*h*/*B* = 15) is considered for this purpose as it is most

representative of geometries likely to be encountered in practice (Royston 2018; Royston et al. 2020). It is noteworthy that any resulting bias is on the conservative side for this problem. It is found empirically that the following expression can be used to capture the bearing capacity factor for a plane-strain cutting face:

$$N'_{R=\infty} = 1366 \cdot \tanh([94.2x - 768.3y + 674.3] \times 10^{-2}) + 2.8$$

$$x = \tanh([28.2\alpha - 14.7\beta - 217.9\phi'] \times 10^{-3} + 10.87) \quad (4)$$

$$y = \tanh([-25.8\alpha - \beta - 14.58\phi'] \times 10^{-2} + 8.62)$$

where both β and ϕ′ are defined in degrees and tanh functions are used to capture the non-linearity in the data. Equation (4) was used to re-calculate the bearing capacity of all plane strain analyses considered in the preceding parameteric study; the results are compared to the FELA output in Fig. 15 where good agreement can be observed.

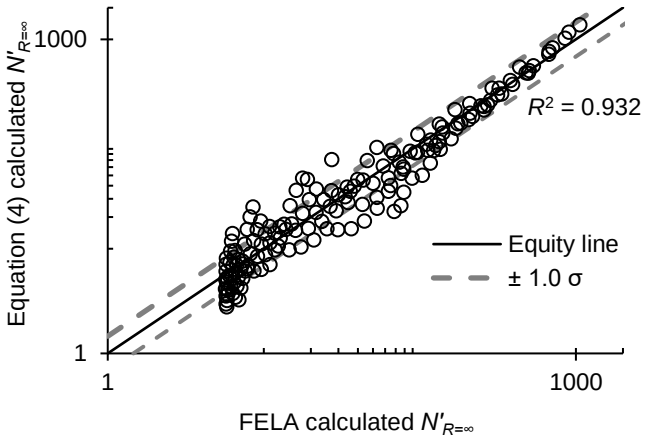

Fig. 15 Comparison between calculated values of the plane strain bearing capacity factor, $N'_{R=\infty}$ determined using equation (4) and FELA (*h/B* = 15 only); σ = standard deviation.

Recognising that the logarithm of $N'/N'_{R=\infty}$ was shown to vary approximately linearly with *B/R* (see Fig. 13), the following expression was used to extend equation (4) to axisymmetric conditions:

$$N' = \exp\left[m\left(\frac{B}{R}\right)\right] N'_{R=\infty} \quad (5)$$

where the curve-fitting parameter *m* represents the gradient of the data in the parameter space shown in Fig. 13. An expression for *m* was developed by fitting a linear relationship to these data and further regressing the fitted slope on the parameters α, β and ϕ′. This exercise yielded the following expression:

$$m = \exp([78.9\phi' + 327\alpha - 2301] \times 10^{-3}) \quad (6)$$

Figure 16 compares calculations determined using equations (4) – (6) to the FELA output for all 6300 parameter combinations, including both plane strain and axisymmetric conditions. While there is generally good agreement between both sets of calculations, the present analytical approach provides a slight over-prediction at low bearing capacities compared to the FELA output. While this agreement can be improved further by introducing additional non-linearity in the present analytical equations (particularly equations (5) and (6)) this leads to a significant increase in model complexity. The proposed model was therefore adopted as a reasonable balance between fidelity and complexity.

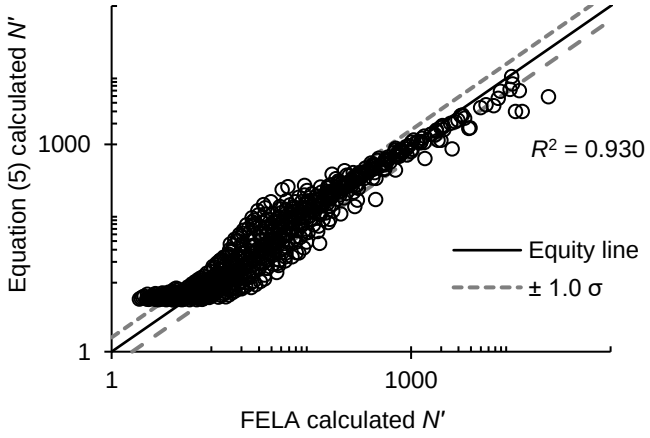

Fig. 16 Comparison between calculated values of the bearing capacity factor, *N′* determined using equation (5) and FELA for all analyses with *h/B* = 15; σ = standard deviation.

Limitations of method

Modelling of drained materials is a complex problem and assumptions imposed in the modelling have important implications for future applications of the proposed design method. Firstly, the authors recognise that a non-linear failure envelope provides a better prediction of the shear strength of sands, particularly at low confining pressures (Bolton 1986). The FEA results show that soil associativity has a significant influence on the bearing capacity for this problem and the use of associated flow is likely to provide an over-estimate of the bearing capacity when applied to practical problems (e.g. Loukidis and Salgado, 2009). An overestimate of caisson bearing resistance may lead to uncontrolled sinking or 'runaway' (i.e. caisson sinks too far ahead to place next level of wall shuttering). These risks can be managed on site by, for example, flooding the caisson to avail of additional buoyant uplift forces or deploying 'brakes' on the top supporting ring beam. However, the primary risk in caisson construction is failure to sink to formation level arising from an underestimate of the soil penetration resistances (to the point where they exceed the self-weight of the structure). The resulting bias of the present calculations are therefore on the safe side for this problem such that these results may be transferred to practice with confidence.

Finally, several authors have reported scale effects (due to the pressure dependence of the bearing capacity on ϕ') and therefore a dependence of the bearing capacity on the width of the foundation (Griffiths 1982, Cerato and Luteneggar 2007) which has not been considered here. The design method described in this paper assumes that an adequate assessment of these issues has been completed.

CONCLUSIONS

This paper has described a numerical study of the vertical bearing capacity of a caisson cutting face embedded in cohesionless soil. Finite element limit analyses were used to explore the role of the cutting face inclination angle, roughness, external embedment depth

435 and radius on the vertical soil reaction. A limited number of additional calculations were
436 completed using finite element analysis to assess the role of soil non-associativity on the
437 vertical bearing capacity.

438 The parametric study revealed that the influence of the cutting face inclination angle on the
439 bearing capacity is highly dependent on both the soil friction angle and the roughness of the
440 cutting face. For a rough cutting face, a steepening of the inclination angle was shown to
441 increase the vertical bearing capacity for all values of ϕ'. In contrast, for a smooth interface,
442 a steepening of the cutting face caused an increase in the bearing capactity for low-ϕ' soil
443 and a reduction for high-ϕ' soil. The results also revealed the existence of a critical external
444 embedment depth beyond which any further increases in embedment had a negligible
445 influence on the bearing capacity. Finally, a reduction in the caisson radius was shown to
446 cause a significant increase in the bearing capacity due to an increase in radial stress, and
447 therefore confining stress, in the soil towards the internal side of the caisson wall. The role of
448 the caisson radius on the bearing capacity was largely controlled by the soil friction angle
449 where high-ϕ' soil exhibited a greater dependency on the caisson radius.

450 The numerical output was used to inform the development of closed-form design
451 calculations for the vertical penetration resistance of large-diameter open caissons
452 embedded in cohesionless soils. The equations were shown to provide a very good
453 approximation of the numerical results and are amenable for use in routine design.

454 In this study, simplifying assumptions have necessarily been adopted to numerically model
455 the caisson sinking problem in sand. In particular, the use of associated flow is likely to
456 provide an over-estimate of caisson bearing capacity which may lead to uncontrolled sinking
457 or ‘runaway’ (i.e. caisson sinks too far ahead to place next level of wall shuttering). However,
458 these risks can be managed on site by, for example, flooding the caisson to avail of
459 additional buoyant uplift forces or deploying ‘brakes’ on the top supporting ring beam.

460 Nevertheless, the present results suggest interesting soil-structure interaction behaviours at
461 the caisson cutting face. Further experimental validation of the presented results and the

developed design methodology is clearly desirable to inform future developments considering, for example, large deformation effects, soil non-associativity, and stress- and density-dependency.

ACKNOWLEDGMENTS

This project was supported by the Royal Academy of Engineering under the Research Fellowship Scheme and the Engineering and Physical Sciences Research Council (grant no. EP/T006900/1).

REFERENCES

Abbo, A.J., Lyamin, A.V., Sloan, S.W., Hambleton, J.P., 2011. A C2 continuous approximation to the Mohr–Coulomb yield surface. Int. J. Solids Struct. 48, 3001–3010. https://doi.org/10.1016/j.ijsolstr.2011.06.021

Benmebarek, S., Remadna, M.S., Benmebarek, N. and Belounar, L., 2012. Numerical evaluation of the bearing capacity factor Nγ′ of ring footings. *Computers and Geotechnics*, *44*, pp.132-138.

Benmebarek, S., Saifi, I. and Benmebarek, N., 2017. Undrained vertical bearing capacity factors for ring shallow footings. *Geotechnical and Geological Engineering*, *35*(1), pp.355-364.

Bolton, M.D., 1986. The strength and dilatancy of sands. *Geotechnique*, *36*(1), pp.65-78.

Boushehrian JH, Hataf N. Experimental and numerical investigation of the bearing capacity of model circular and ring footings on reinforced sand.Geotext Geomembr 2003;21:241–56.

Brinch Hansen, J. (1970). A revised and extended formula for bearing capacity, Bulletin No. 28. Lyngby: Danish Geotechnical Institute.

Cassidy, M.J. and Houlsby, G.T., 2002. Vertical bearing capacity factors for conical footings on sand. *Géotechnique*, *52*(9), pp.687-692.

Cerato, A.B. and Lutenegger, A.J., 2007. Scale effects of shallow foundation bearing capacity on granular material. *Journal of Geotechnical and Geoenvironmental Engineering*, *133*(10), pp.1192-1202.

Chavda, J.T., Mishra, S. and Dodagoudar, G.R., 2019. Experimental evaluation of ultimate bearing capacity of the cutting edge of an open caisson. *International Journal of Physical Modelling in Geotechnics*, pp.1-14.

Choobbasti AJ, Hesami S, Najafi A, Pirzadeh S, Farrokhzad F, Zahmatkesh A. Numerical evaluation of bearing capacity and settlement of ring footing, casestudy of Kazeroon cooling towers. Int J Res Rev Appl Sc 2010;4(3):263–71

Dassault Systèmes, 2017. Abaqus FEA.

De Beer, E. E. (1970). Experimental determination of the shape factors and the bearing capacity factors of sand. *Géotechnique* 20, No. 4, 387–411.

De Borst, R. and Vermeer, P.A., 1984. Possibilites and limitations of finite elements for limit analysis. *Geotechnique*, *34*(2), pp.199-210.
Drescher, A. and Detournay, E., 1993. Limit load in translational failure mechanisms for associative and non-associative materials. *Géotechnique*, *43*(3), pp.443-456.
Georgiadis, K., 2010. An upper-bound solution for the undrained bearing capacity of strip footings at the top of a slope. *Géotechnique*, *60*(10), pp.801-806.
Goss, C.M. and Griffiths, D.V., 2001. Rigorous plasticity solutions for the bearing capacity of two-layered clays. *Geotechnique*, *51*(2), pp.179-183.
Gourvenec, S., 2007. Shape effects on the capacity of rectangular footings under general loading. *Géotechnique*, *57*(8), pp.637-646.
Griffiths, D.V., 1982. Computation of bearing capacity factors using finite elements. *Geotechnique*, *32*(3), pp.195-202.
Hansen, J. B. (1970). A revised and extended formula forbearing capacity, Bulletin 28, pp. 5 - 11. Copenhagen:Danish Geotechnical Institute.
Hjiaj, M., Lyamin, A.V. and Sloan, S.W., 2005. Numerical limit analysis solutions for the bearing capacity factor Nγ. *International Journal of Solids and Structures*, *42*(5-6), pp.1681-1704.
Houlsby, G.T. and Martin, C.M., 2003. Undrained bearing capacity factors for conical footings on clay. *Géotechnique*, *53*(5), pp.513-520.
Krabbenhoft, K., Lyamin, A.V., and Krabbenhoft, A. (2016) OptumG2: Theory. Optum Computational Engineering
Kumar J, Ghosh P. Bearing capacity factor Nγ for ring footings using the method of characteristics. Can Geotech J 2005;42:1474–84.
Lee, J.K., Jeong, S. and Lee, S., 2016. Undrained bearing capacity factors for ring footings in heterogeneous soil. *Computers and Geotechnics*, *75*, pp.103-111.
Loukidis, D. and Salgado, R., 2009. Bearing capacity of strip and circular footings in sand using finite elements. *Computers and Geotechnics*, *36*(5), pp.871-879.
Lyamin, A.V., Salgado, R., Sloan, S.W. and Prezzi, M., 2007. Two-and three-dimensional bearing capacity of footings in sand. *Géotechnique*, *57*(8), pp.647-662.
Martin, C.M., 2011. The use of adaptive finite-element limit analysis to reveal slip-line fields. Géotechnique Lett. 1, 23–29. https://doi.org/10.1680/geolett.11.00018
Merifield, R.S., Sloan, S.W. and Yu, H.S., 1999. Rigorous plasticity solutions for the bearing capacity of two-layered clays. *Geotechnique*, *49*(4), pp.471-490.
Meyerhof, G. G. (1951). The ultimate bearing capacity of foundations. *Géotechnique*, 2(4), 301–332.
Meyerhof, G. G. (1963). Some recent research on bearing capacity of foundations. *Can. Geotech. J.* (1)1, 16–26.
Michalowski, R.L., 2001. Upper-bound load estimates on square and rectangular footings. *Géotechnique*, *51*(9), pp.787-798.
Royston, R., Phillips, B., Sheil, B.B. and Byrne, B.W. (2016) Bearing capacity beneath tapered blades of open dug caissons in sand. *Civil Engineering Research in Ireland (CERI), Galway, Ireland.*
Royston, R., Sheil, B.B. and Byrne, B.W. (2020) Monitoring the construction of a large-diameter caisson in sand. *Proceedings of the ICE - Geotechnical Engineering*. Accepted.
Saha MC. Ultimate bearing capacity of ring footings on sand. M. Eng. Thesis. UP,India: University of Roorkee, Roorkee; 1978.
Salgado, R., Lyamin, A.V., Sloan, S.W. and Yu, H.S., 2004. Two-and three-dimensional bearing capacity of foundations in clay. *Géotechnique*, *54*(5), pp.297-306.
Saran S, Bhandari NM, Al-Smadi MMA. Analysis of eccentrically–obliquely loaded ring footings on sand. Ind Geotech J 2003;33(4):422–46.

552 Sastry, V.V.R.N. and Meyerhof, G.G., 1987. Inclination factors for strip footings. *Journal of*
553 *geotechnical engineering*, *113*(5), pp.524-527.
554 Sheil, B.B., Royston, R. and Byrne, B.W. (2018) Real-time monitoring to inform the
555 construction of large-diameter caissons. *China-Europe Conference*
556 Shewchuk, J.R., 2002. Delaunay refinement algorithms for triangular mesh generation.
557 Comput. Geom. 22, 21–74. https://doi.org/10.1016/S0925-7721(01)00047-5
558 Shewchuk, J.R., 1996. Triangle: Engineering a 2D quality mesh generator and Delaunay
559 triangulator, in: Applied Computational Geometry: Towards Geometric Engineering,
560 Lecture Notes in Computer Science. Presented at the Workshop on Applied
561 Computational Geometry, pp. 203–222. https://doi.org/10.1007/BFb0014497.
562 SIMULIA (2017) Abaqus User Documentation 2017. Providence, RI, USA: Dassault
563 Systèmes Simulia Corp.
564 Sloan, S.W., Abbo, A.J., Sheng, D., 2001. Refined explicit integration of elastoplastic models
565 with automatic error control. Eng. Comput. 18, 121–154.
566 https://doi.org/10.1108/02644400110365842
567 Sloan, S.W., 2013. Geotechnical stability analysis. Géotechnique, 63(7), pp.531-571.on
568 Geotechnical Engineering, Vienna, Austria.
569 Smith, C.C., 2005. Complete limiting stress solutions for the bearing capacity of strip footings
570 on a Mohr-Coulomb soil. *Géotechnique*, *55*(8), pp.607-612.
571 Taiebat, H.A. and Carter, J.P., 2010. A failure surface for circular footings on cohesive
572 soils. *Géotechnique*, *60*(4), pp.265-273.
573 Terazaghi, K., 1965. Theoretical soil mechanics. *John Wiley and Sons*.
574 Van Baars, S., 2014. The inclination and shape factors for the bearing capacity of
575 footings. *Soils and Foundations*, *54*(5), pp.985-992.
576 Vermeer, P.A., 1990. The orientation of shear bands in biaxial tests. *Geotechnique*, *40*(2),
577 pp.223-236.
578 Vesic, A. S. (1973). Analysis of ultimate loads of shallow foundations. J. Soil Mech. Div.
579 ASCE 99, No. SM1, 45–73.
580 Zhao L, Wang JH. Vertical bearing capacity for ring footings. Comput Geotech
581 2008;35(2):292–304.